Performance studies of a lead-scintillation fiber calorimeter prototype for the linear collider detector

K. Ishii[a], I. Nakamura[a], Y. Fujii[c], F. Kajino[b], J. Kanzaki[c], K. Kawagoe[a], Y. Kurihara[c], K. Nagai[a, †], M. Nozaki[a], T. Okubo[b], Y. Sugimoto[b], H. Takeda[a], S. Tanaka[a], K. Taruma[a, ††], Y. Yamaoka[c], C. Yokoyama[a]

[a] Faculty of Science, Kobe University, Kobe, Hyogo, Japan
[b] Faculty of Science, Konan University, Kobe, Hyogo, Japan
[c] KEK, National Laboratory for High Energy Physics, Tsukuba, Ibaraki, Japan

Abstract

We constructed calorimeter modules composed of lead plates and scintillating fibers as an R & D program for the experiment at a future electron-positron linear collider. We tested the performance of the modules using electron and pion beams at the KEK proton synchrotron. The results of the beam tests are presented in this paper.

1 Introduction

Several groups have recently proposed construction of electron-positron linear colliders with center of mass energies 300-500 GeV [1, 2]. Physics goals at such a future linear collider include detection and study of the Higgs boson, detailed study of the top quark, and precision tests of the electroweak theory. We also have a good chance to explore new physics beyond the standard model. In order to achieve the physics goals at the future linear collider, we have to construct a detector with an excellent energy/momentum resolution and a good hermeticity, as well as with efficient b-tagging and lepton-identification capabilities. Calorimeter is one of the most important components of the detector. The resolution of the invariant mass of hadronic jets is essential in most of the physics studies. To this purpose the calorimeter should have excellent energy resolutions both for electromagnetic and hadronic showers. A good hermeticity of the calorimeter is also required to measure the missing energy and momentum carried by neutrinos or other weakly interacting particles such as the lightest neutralinos in SUSY models.

Calorimeter modules composed of LEad plates and Scintillating FIbers [3-10], which we hereafter call LESFI, can be one of the realistic candidates because of the following reasons.

[†] Now at The Weizmann Institute of Science, Rehovot, Israel
[††] Now at Osaka University of Commerce, Osaka, Japan

- Because of the use of scintillation fibers as the active component fine sampling is easily obtained, resulting in a good energy resolution both for electromagnetic and hadronic showers [3, 7, 8].

- It is known that equal response to electromagnetic and hadronic showers can be realized by adjusting the volume ratio of the lead plates and scintillating fibers. This leads to a good energy resolution for hadronic showers [11-13].

- Because the LESFI modules can measure energies of the electromagnetic and hadronic showers simultaneously, and also because lead plates are used as the absorber, the calorimeter is relatively compact in size. Therefore it is possible to locate the whole calorimeter in the solenoidal magnet so that good hermeticity can be easily achieved. The material in front of the calorimeter, which may degrade the calorimeter performance, can also be much reduced.

We constructed test modules of the LESFI calorimeter and tested their performance using electron and pion beams at the KEK proton synchrotron. Results of the beam tests are presented in the following sections.

2 Test Modules

A schematic drawing of the LESFI test modules is shown in Fig. 1. Lead plates of 2 mm thickness, containing 6% antimony in weight for hardness, were machined to have parallel grooves with intervals of 2.2 mm. Each plate has a dimension of 100×1300 mm^2. Polystyrene-based scintillating fibers (KURARAY SCSF-38) of 1 mm in diameter were embedded in all of the grooves. The fibers were approximately 1.5 m long, longer than the lead plates. The volume ratio of the lead plates and scintillating fibers was chosen to be about 4:1 with which we expected the equal response to electromagnetic and hadronic showers. The refractive indices of the polystyrene core and the PMMA (Poly-MetylMethAcrylate) clad were 1.59 and 1.49, respectively. The side surfaces of the fibers were painted with white reflector (NE560) in order to improve the light collection efficiency. The attenuation length of the scintillation light in the fibers was measured to be roughly 3000 mm.

The lead plates with fibers were stacked to form a mini-module with a cross section of 100×50 mm^2. At the front end of the mini-module, the cross sections of the fibers were polished and then were painted with the white reflector. At the rear end the fibers were grouped into two bundles. The end of each bundle was cut and polished to make a flat surface. An acrylic light guide was glued to the end surface of the bundle and then a photomultiplier tube (Hamamatsu R1355) was glued to the light guide. We defined a LESFI segment as the region which a photomulitiplier (or a bundle) covered. A segment corresponded to a cross section of 50×50 mm^2. A total of eight mini-modules were assembled to make a module of 200×200 mm^2 cross section. The average radiation length (X_0) and the interaction length (λ_0) of the LESFI material were calculated to be 7.5 mm and 210 mm, respectively. The length of the LESFI modules corresponded to 173 X_0 and 6.2 λ_0.

3 Beam Test

The LESFI modules were tested at the $\pi 2$ beam line of the KEK proton synchrotron. The available momentum was about 4 GeV/c at maximum. The electron/pion ratio in the beam was about 1/1000 in population.

Fig. 2 shows the schematic view of the setup at the beam test. We set two trigger counters, TR1 and TR2, in front of a movable stage on which the LESFI modules were mounted. Each of the trigger counters was a scintillation counter with a cross section of 50 $\times$ 50 mm^2, and the distance between the two counters was about 2800 mm. Between the trigger counters were two gas Čerenkov counters, CH1 and CH2, to identify electrons in the beam. In taking electron data, we used the coincidence of TR1, TR2, CH1 and CH2 signals as the event trigger. On the other hand, we used the coincidence of only TR1 and TR2 signals as the event trigger in taking pion data. We removed the electron contamination in the pion data by the offline analysis.

For the determination of the incident position of the particles, we set two drift chambers, DC1 and DC2, between the TR2 counter and the movable stage. Each of the chambers could measure both vertical and horizontal positions. The cross section of the drift chambers was 200 $\times$ 200 mm^2, and the extrapolated position resolution was about 2 mm at the front surface of the LESFI modules.

In addition to the LESFI modules, the following detectors were mounted on the movable stage.

- Leakage shower counters (hereafter we call them LEAK) which surrounded the LESFI modules. The counters were sandwich-type calorimeter, consisting of 10 mm thick lead plates and 2.5 mm thick scintillator plates. The scintillation light was collected into two photomultipliers through two wavelength shifter plates of 2 mm thickness. The active volume of a LEAK counter was 385 $\times$ 186 $\times$ 1000 mm^3, and the length corresponded to 133 X_0 and 4.8 λ_0.

- Preshower detector (hereafter we call it PSD) located in front of the LESFI modules. The PSD was also sandwich-type, and consisted of six layers of a 4 mm thick lead plate and a 1 mm thick scintillator plate, resulting in a total thickness of 4 X_0. The scintillation light was led into four photomultipliers through two wavelength shifter plates of 4 mm thickness.

All the signals from the calorimeters and the trigger counters were fed into 12 bit FASTBUS ADC modules. The ADC channels had two different ranges, resulting in an effective dynamic range of 15 bit. The timing signals of the drift chambers were fed into FASTBUS TDC modules with an effective dynamic range of 15 bit. One bit of TDC corresponded to 100 ps. Once an event was triggered, all the data were read out and recorded by a personal computer.

We took various data changing the beam momentum and the setup of the detectors. The beam momentum was set to be 1.0 , 1.5 , 2.5 and 4.0 GeV/c. The stage could move horizontally and vertically, as well as rotate in the horizontal plane. The incident position and the horizontal angle (θ_x) of the beam to the LESFI modules were changed with the movable stage. The data without the PSD were also taken.

4 Results

In the following analysis only the events which had only one single track were used. They were selected with the following conditions.

- Each of the trigger counters (TR1 and TR2) had the signal consistent with the passage of a minimum ionizing particle. (see Fig. 3(A) and (B))
- Each of the drift chambers (DC1 and DC2) had only one hit.

The offline selections by the Čerenkov signals were also applied to electron and pion data for higher purity. The scatter plots of the Čerenkov signals are shown in Fig. 3(C) and (D).

The gain of each segment in the LESFI modules was calibrated with electrons, where the electrons of 1.0, 1.5, and 2.5 GeV/c were incident to the central region of the corresponding segment, with an incident angle of $\theta_x = 3^\circ$. The deviation from the fitted linear response was found to be within 1.2%. The LEAK counters were calibrated in a similar way, but with the angle of $\theta_x = 0^\circ$.

4.1 Energy Resolution for Electrons

To evaluate the energy resolution for electrons we used only the events in which electrons entered to the central region (20×20 mm^2) of the front surface of a segment. The total energy of the LESFI modules (E_{LESFI}) was defined as the sum of the signals of the central segment and its eight surrounding ones. About 92% of the total energy was deposited in the central segment on average. In the case where the PSD was located in front of the LESFI modules, the total energy (E) is calculated with the following formula,

$$E = \alpha \times E_{PSD} + E_{LESFI},$$

where E_{PSD} is the energy deposit measured in the PSD. The coefficient α was determined at each energy point such that the best energy resolution was obtained. For the data without the PSD, E_{LESFI} is simply used as the total energy. An example of the total energy distribution is shown in Fig. 4, together with those of the PSD and the LESFI.

By fitting the total energy distribution to a Gaussian function, we obtained the energy resolution for electrons. The results at $\theta_x = 3^\circ$ with and without the PSD are given in Table 1 and are also shown in Fig. 5. The resolutions can be expressed in the following formulae;

$$\begin{aligned} \frac{\sigma_E}{E} &= \frac{(14.4 \pm 0.3)\ \%}{\sqrt{E(\mathrm{GeV})}} \oplus (0.0 \pm 1.4)\ \% \quad \text{without the PSD,} \\ &= \frac{(14.7 \pm 0.4)\ \%}{\sqrt{E(\mathrm{GeV})}} \oplus (0.0 \pm 1.8)\ \% \quad \text{with the PSD,} \end{aligned}$$

where $\oplus$ means a quadratic sum defined as

$$\sqrt{\left(\frac{A}{\sqrt{E}}\right)^2 + B^2},$$

where A and B correspond to coefficient of $\mathrm{E}^{-1/2}$ and constant term, respectively.

We made a Monte Carlo simulation of the beam test with a program based on GEANT3. The energy resolutions obtained by the Monte Carlo simulation are also given in Table 1 and in Fig. 5. The resolutions can be expressed in the following formulae;

$$\begin{aligned}\frac{\sigma_E}{E}_{(sim.)} &= \frac{(13.9 \pm 0.5)\ \%}{\sqrt{E(\mathrm{GeV})}} \oplus (2.9 \pm 1.0)\ \% \quad \text{without the PSD,} \\ &= \frac{(14.3 \pm 0.2)\ \%}{\sqrt{E(\mathrm{GeV})}} \oplus (0.0 \pm 1.6)\ \% \quad \text{with the PSD.}\end{aligned}$$

The experimental and simulation results are consistent with each other.

Energy resolution for electrons depends on the angle θ_x between the incident particle and the fiber direction. According to previous studies [3], the energy resolution deteriorates quite rapidly for small incident angles ($\theta_x < 2°$) at 40 GeV. It is considered that the angular dependence is originated from the fact that at small incident angles the signal of the particle hitting directly the fiber is much larger than that hitting the lead. Fig. 6(A) shows a simulation result for the dependence of the signal on the incident position of electrons. We clearly see the position dependence for $\theta_x = 0°$ in the simulation. In the case of small incident angles the position dependence gives the energy distribution a higher tail and the distribution deviates from a Gaussian. The energy distribution of the experimental data at θ_x = 0° is shown in Fig. 6(C). For incident angles greater than 2°, however, the position dependence is not so significant and the signal distribution looks a perfect Gaussian. The angular dependence of the energy resolution is shown both for experimental and simulation data in Fig. 6(E). Locating the PSD in front efficiently reduces the angular dependence, because of the shower development before entering the LESFI modules. Similar plots with the PSD in front are shown in Fig. 6(B),(D) and (F), where no significant position dependence was observed, as expected.

4.2 Position Resolution for Electrons

The incident position of electrons can be determined by the energy sharing among the LESFI modules. We first calculated the position (x, y) as the weighted average of the center positions of the LESFI segments;

$$\begin{aligned}x &= \frac{\sum_i x_i E_i}{\sum_i E_i}, \\ y &= \frac{\sum_i y_i E_i}{\sum_i E_i},\end{aligned}$$

where (x_i, y_i) and E_i denote the center position and the energy deposit of i'th segment, respectively. The x-direction and y-direction were defined to be horizontal and vertical. Fig. 7(A) and (B) show the scatter plots of the incident positions measured by the drift

chambers and the LESFI modules, where the electrons of 4.0 GeV/c were incident with an incident angle of θ_x = 3°. The data without the PSD were used in this analysis.

It is known that the position calculated as above needs further correction. We used the tangent-shape function for this correction, as shown by the solid line in the figures. Fig. 7(C) and (D) show the distributions of the difference between the corrected position and the position measured by the drift chambers. We obtained the position resolutions of the LESFI modules by fitting the distributions to Gaussians. The results at $\theta_x = 3°$ are summarized in Table 2 and shown in Fig. 8.

The dependence of the position resolution on the electron energy can be expressed as

$$\sigma_x = \frac{(6.6 \pm 0.8)\ \text{mm}}{\sqrt{E(\text{GeV})}} \oplus (1.5 \pm 1.8)\ \text{mm} \quad \text{at } \theta_x = 3°,$$

$$\sigma_y = \frac{(5.6 \pm 0.8)\ \text{mm}}{\sqrt{E(\text{GeV})}} \oplus (2.4 \pm 1.0)\ \text{mm} \quad \text{at } \theta_x = 3°.$$

The position resolutions expected from the Monte Carlo simulation are also given in Table 2 and shown in Fig. 8, where the incident positions were uniformly distributed over a segment surface in the simulation. Simulation results can be expressed as

$$\sigma_{x(sim.)} = \frac{(6.4 \pm 0.3)\ \text{mm}}{\sqrt{E(\text{GeV})}} \oplus (2.2 \pm 0.4)\ \text{mm} \quad \text{at } \theta_x = 3°,$$

$$\sigma_{y(sim.)} = \frac{(6.1 \pm 0.3)\ \text{mm}}{\sqrt{E(\text{GeV})}} \oplus (2.1 \pm 0.3)\ \text{mm} \quad \text{at } \theta_x = 3°.$$

The experimental results agreed well with those of the simulation.

The angular dependence of the position resolution was also studied using the data of 4.0 GeV/c electrons without the PSD in front at incident angles of $\theta_x = 0°, 3°, 6°$ and 9°. We observed no significant angular dependence in the data.

4.3 Energy Resolution for Pions

We used pion data with an incident angle of $\theta_x = 0°$ to obtain the energy resolution for pions, because we expected a very small angular dependence for pions [6]. The contamination of electrons in the data was removed using information of Čerenkov signals in the offline analysis. We defined the total energy as the sum of all the signals from the LESFI modules and the LEAK counters. As in the case for electrons, $\alpha \times E_{PSD}$ was added to the total energy when the PSD was located in front. An example of the total energy distribution is shown in Fig. 9. The energy resolutions at various energy points are listed in Table 3 and are shown in Fig. 10 together with those of Monte Carlo simulations. In the simulation we used the FLUKA package for hadron interaction. However, the simulation did not describe the experimental data well. We tried to use other package (GHEISHA), but the results did not agree with the experimental data either. This suggests that the simulators for the hadronic

showers are still to be optimized for low energy hadronic interactions. The energy resolution for pions can be expressed by the following formulae;

$$\frac{\sigma_E}{E}_{(exp.)} = \frac{(38.1 \pm 1.3)\ \%}{\sqrt{E(\mathrm{GeV})}} \oplus (11.6 \pm 1.4)\ \% \text{ without the PSD},$$

$$\frac{\sigma_E}{E}_{(exp.)} = \frac{(37.2 \pm 1.6)\ \%}{\sqrt{E(\mathrm{GeV})}} \oplus (15.8 \pm 1.4)\ \% \text{ with the PSD},$$

$$\frac{\sigma_E}{E}_{(sim.)} = \frac{(34.3 \pm 1.7)\ \%}{\sqrt{E(\mathrm{GeV})}} \oplus (13.8 \pm 2.0)\ \% \text{ without the PSD},$$

$$\frac{\sigma_E}{E}_{(sim.)} = \frac{(32.2 \pm 1.7)\ \%}{\sqrt{E(\mathrm{GeV})}} \oplus (18.5 \pm 1.6)\ \% \text{ with the PSD}.$$

The large constant term seems due to the lateral shower leakage from the LESFI modules and the LEAK counters. By comparing the lateral shower profile with that of the previous experiment [5], it was estimated that about 5 % of energy escaped from the lateral sides of our test modules.

The signal ratio for electrons and pions is obtained to be

$$\frac{A_e}{A_\pi} = 1.19\ .$$

The A_e and A_π are the coefficients determined from the linearity ($E = A \times E_{inc}$) between the incident energy E_{inc} and the measured total energy E for electrons and pions respectively, where we took account of the shower leakage mentioned above. Similar to the result from the other group [5], our data suggests that the test modules, in which the volume ratio of lead to fiber was set to approximately 4:1, does not give exactly equal response to electromagnetic and hadronic showers.

4.4 Electron Identification

We can distinguish electrons from charged hadrons by utilizing the difference of the lateral shower profiles of electromagnetic and hadronic showers in the LESFI modules. The signal from the PSD can be used as another tool for electron identification. As the PSD signal is almost independent of the lateral shower profile, electron identification can be much improved if they are combined.

We may also distinguish electrons from charged hadrons by utilizing the difference in time structure between electromagnetic and hadronic showers in the LESFI modules. To this purpose we made special runs where the signals from the LESFI modules were fed into a digital oscilloscope of 2 GS/s rate without the PSD. In addition to the ordinary LESFI modules, we constructed a double-ended mini-module which had a light guide and a photomultiplier tube at both ends, and studied the time structures of the signals from both ends.

4.4.1 The Lateral Shower Profile and the PSD Signal

We defined two parameters which characterized the lateral shower profile in the LESFI modules. One is the containment parameter C defined as

$$C = \frac{\sum_i E_i \quad (i\ ;\ Central\ 9\ Segments)}{\sum_j E_j \quad (j\ ;\ LESFI\ +\ LEAK)}\ ,$$

where E_i denotes the energy deposit in i'th LESFI segment. The suffix i runs over the central segment and its eight surrounding ones, while the suffix j runs over all of the LESFI segments and the LEAK counters. The other is the lateral shower spread S defined as

$$S = \frac{\sum_i D_i^2 E_i}{\sum_i E_i},$$

where D_i is the distance between the incident position determined by the drift chambers and the central position of i'th segment. Fig. 11 shows the distributions of C and S values for electrons and pions of 2.5 GeV/c.

Fig. 12(A) and (B) show the distributions of the energy deposit in the PSD for electrons and pions of 2.5 GeV/c, respectively. The distribution for pions has a narrow peak which corresponds to the passage of a single minimum ionizing particle. The energy deposit for electrons is much larger on average and has a much broader distribution, because of the development and the fluctuation of electromagnetic showers in the PSD. The scatter plots of the PSD signal and C or S values are shown in Fig. 12(C) and (D).

We define the electron efficiency and the pion rejection factor as;

$$\begin{aligned} \text{Electron efficiency} &= \frac{N_e^{SEL}}{N_e^{ALL}}, \\ \text{Pion rejection factor} &= \frac{N_\pi^{ALL}}{N_\pi^{SEL}}, \end{aligned}$$

where N^{ALL} and N^{SEL} are the number of all single-track events and the number of events selected as electrons from the single-track events, respectively. In order to compare the methods for electron identification, we calculate the pion rejection factors with various selection cuts for fixed electron efficiencies. They are summarized in Table 4. In spite of relatively low particle momentum in the beam test, the LESFI modules were found to have sufficiently high rejection factors against pions. The rejection factor is especially high if the LESFI modules are used in combination with the PSD.

4.4.2 Electron Identification from Time Structure

Some differences are expected between the time structures of electromagnetic and hadronic showers. The differences originate from the following characteristics of showers.

1. As the longitudinal shower spread is generally larger for hadronic shower than for electromagnetic shower, the former tends to have broader pulse width.

2. The effect of the neutron component in hadronic shower appears as a long tail in the signal timing.

3. The depth of the maximum shower point is shorter for electromagnetic showers than for hadronic showers. Therefore for electromagnetic showers, the arrival time of the scintillation light to the front end is much earlier than that to the rear end of a calorimeter module.

We use the pulse width as the variable which characterize the first and second items above. The pulse width was defined as the fall time from 90 % peak to 40 % peak for the ordinary LESFI modules and from 95 % peak to 45 % peak for the double-ended mini-module, respectively, such that the best separation power was obtained. Fig. 13 shows the distributions of the pulse widths for electrons and pions of 4.0 GeV/c with the ordinary LESFI modules and the double-ended mini-module. For the ordinary LESFI modules, the particles were incident to the central region of a segment with an incident angle of $\theta_x = 3°$. On the other hand, for the double-ended mini-module, the particles were incident to the edge area of a segment with $\theta_x = 6°$, in order that they did not hit the light guide and the photomultiplier tube at the front end. Because of the difference in the incident angles the distribution of the electron pulse widths were broader for the double-ended mini-module, and the pion rejection factor was degraded. The electron efficiency and the pion rejection factor are summarized in Table 5 and 6.

The time difference of the signals at the front end and the rear end was used to characterize the third item. The distributions of the time difference with the double-ended mini-module are superposed in Fig. 14. The timing difference is almost independent of the pulse width. The scatter plot of the pulse width and the time difference is also shown in Fig. 14. The resulting electron efficiency and pion rejection factor are listed in Table 6.

According to D. Acosta *et al.* [4] the time structure (pulse width) has high sensitivity in separating electrons from pions. They reported that the pion rejection factor of more than 1000 was obtained at the energy of 80 GeV by the analysis of the pulse width. On the other hand, the other group [9] reported that no separation can be obtained by timing discrimination at the low energy (below 10 GeV). However, their detector was too short (only 1.32 interaction lengths) to detect the difference of the longitudinal shower spread and the existence of the neutron component. Our result firstly demonstrated the possibility to separate electrons from pions even at low energies, although the sensitivity is rather low compared to the results at higher energy region.

5 Summary

A sampling calorimeter consisting of 1 mm diameter scintillation fibers embedded in lead plates was constructed and tested for electrons and pions of momentum between 1.0 GeV/c and 4.0 GeV/c.

The energy resolution for electrons was measured to be $14\%/\sqrt{E(\mathrm{GeV})}$ plus a sufficiently small constant term with and without the preshower detector. The position resolution for

electrons was measured to be roughly 6 mm$/\sqrt{E(\mathrm{GeV})}$. The energy resolution for pion was measured to be 38%$/\sqrt{E(\mathrm{GeV})}$ plus 12 % constant term. This large constant term is assumed to be caused by incomplete containment of hadronic showers. Various ways to distinguish electrons from pions were investigated. Even at the low energy, the separation by using the lateral shower spread was found to be sufficiently good. The LESFI modules showed good performance in electron identification if they were used together with the preshower detector. The separation between electromagnetic showers and hadronic showers was demonstrated by using the time structure of showers, although the rejection factor is small compared to that at higher energies.

Acknowledgment

We would like to thank the members of the beam-channel group of the KEK proton synchrotron for their kind support during the beam test.

This work was supported, in part, by Grant-in-Aid for Scientific Research from Ministry of Education, Science and Culture under contract No. 04740151.

References

[1] JLC Group, KEK Report 92-16.

[2] DESY 93-123C, Edited by P.M.Zerwas.

[3] D. Acosta et al., Nucl. Instr. and Meth. A294 (1990) 193.

[4] D. Acosta et al., Nucl. Instr. and Meth. A302 (1991) 36.

[5] D. Acosta et al., Nucl. Instr. and Meth. A316 (1992) 184.

[6] The SPACAL Collaboration, CERN/DRDC/90-23.

[7] R. Wigmans, Nucl. Instr. and Meth. A315 (1992) 299.

[8] RD1 Collaboration, Nucl. Instr. and Meth. A344 (1994) 73.

[9] S. Dagoret et al., Nucl. Instr. and Meth. A346 (1994) 137.

[10] H1 SPACAL GROUP, DESY 95-165.

[11] R. Wigmans, Nucl. Instr. and Meth. A259 (1987) 389.

[12] E. BERNARDI et al., Nucl. Instr. and Meth. A262 (1987) 229.

[13] R. Wigmans, CERN-PPE/91-205.

List of Tables

1 The energy resolution σ_E/E (%) for electrons. The results of Monte Carlo simulation are also listed for comparison. 14
2 The position resolution σ_x,σ_y (mm) for electrons. 14
3 The energy resolution σ_E/E (%) for pions. 14
4 The pion rejection factor with various techniques. In case a small number of events were selected for experimental data, we set lower limits at the 95% C.L.. It was denoted by the symbol ">". 15
5 The pion rejection factor with the LESFI modules. The PWD represents the method of the pulse widths. 15
6 The pion rejection factor with the double-ended mini-module. The PWD represents the method of the pulse widths and TD indicates the method of the time difference. 15

List of Figures

1 Schematic drawing of LESFI modules. 16
2 Setup of the beam test. 17
3 The scatter plots showing the signals of trigger counters (TR1 vs. TR2) for 2.5 GeV electrons (A) and pions (B). To remove the double track events we selected the rectangular region as shown in the figure. The scatter plots of gas Čerenkov signals (CH1 vs. CH2) for 2.5 GeV electrons (C) and pions (D) are also shown. The rectangular regions were selected to obtain higher purity. 18
4 The energy distributions for 2.5GeV electrons with the incident angle of $\theta_x = 3°$. The PSD was located in front of LESFI modules. Shown are the energy distributions of the PSD (A) and the LESFI (B), the scatter plot of E_{PSD} versus E_{LESFI} (C) and the corrected total energy distribution (D). . . 19
5 The energy resolution for electrons at $\theta_x = 3°$ without the PSD (A) and with the PSD (B). The filled circles and the solid line show experimental results, while the open squares and the dashed line show results of Monte Carlo simulations. Errors are statistical only. 20
6 The scatter plots of Y-position versus E_{LESFI} by simulation at $\theta_x = 0°$ without the PSD (A) and with the PSD (B), the energy distributions of real data at $\theta_x = 0°$ without the PSD (C) and with the PSD (D) and angular dependence of the energy resolution without the PSD (E) and with the PSD (F). All of the data are for 2.5 GeV electrons. 21
7 The scatter plots showing the position from the LESFI's data versus from the DC's data for x-coordinate (A) and y-coordinate (B). We use the data of 4 GeV electrons at $\theta_x = 3°$ without the PSD. The solid line is the fitting result with tangent-shape function. The residual distributions of corrected x-coordinate (C) and corrected y-coordinate (D) are also shown. 22
8 The position resolution for electrons with the incident angle of $\theta_x = 3°$ without the PSD as a function of the incident energy. Shown are for x-coordinate (A) and y-coordinate (B). The filled circles and the solid line show experimental results, while the open squares and the dashed line show results of Monte Carlo simulations. 23
9 The energy distributions for 2.5GeV/c pions with the incident angle of $\theta_x = 0°$ without the PSD. Shown are the energy distribution of the LEAK (A) and the LESFI (B), the scatter plot of E_{LEAK} versus E_{LESFI} (C) and the combined energy distribution (D). The energy scale is normalized by electron data. 24
10 The energy resolution for pions at $\theta_x = 0°$ without the PSD (A) and with the PSD (B). The filled circles and the solid line show experimental results, while the open squares and the dashed line show results of Monte Carlo simulations. The errors are statistical only. 25

11 The distributions of the lateral shower spread for 2.5 GeV electrons and pions at $\theta_x = 3°$ with the PSD. Shown are C value (see text) for electrons (A), C value for pions (B), S value (see text) for electrons (C) and S value for pions (D). The selection of $C > 0.93$ gives the pion rejection factor of 14.7 with the 95% electron efficiency. The selection of $S < 36.1$ (cm^2) gives the pion rejection factor of 18.7 with the 95% electron efficiency. 26
12 The pulse height distributions of the PSD for 2.5 GeV electrons (A) and 2.5 GeV pions (B). The pion rejection factor of 10.6 with the 95% electron efficiency can be obtained by the cut of PSD < 2150. Scatter plots of the PSD signal versus C value (C) and the PSD signal versus S value (D) are also given. The circle represents the electron data and the open square represents the pion ones. We use the data of 2.5 GeV electrons and pions at $\theta_x = 3°$. The selection of the PSD > 1000 and $C > 0.89$ gives the pion rejection factor of 118 with the 98% electron efficiency. The selection of the PSD > 2000 and $S < 48$ (cm^2) gives pion rejection factor of 202 with the 98% electron efficiency. 27
13 The distributions of the Pulse WiDths (PWD). The data were taken with the digital oscilloscope of 2GS/s. Shown are for 4.0 GeV electrons (A), for 4.0 GeV pions (B) with the ordinary LESFI modules, for 4.0 GeV electrons (C) and for 4.0 GeV pios (D) with the double-ended mini-module. The incident position and angle for the ordinary LESFI modules were the center of the segment and 3° in the horizontal plane. For the double-ended mini-module, the particles were incident to the edge with $\theta_x = 6°$. The selection of $5.6 <$ PWD < 6.7 for the LESFI modules gives the 4.1 pion rejection factor with the 95% electron efficiency. The selection of $4.0 <$ PWD < 6.17 for the double-ended mini-module gives the 2.29 pion rejection factor with the 95% electron efficiency. 28
14 The distribution of Time Differences (TD) of the signals at the front end and the rear end with the double-ended mini-module. Superposed figures are for 4.0 GeV electrons (A) and for 4.0 GeV pions (B). The selection of $6.55 <$ TD < 9.0 gives the pion rejection factor of 2.53 with the 95% electron efficiency. The scatter plot shows the Pulse WiDths (PWD) versus the Time Differences (TD) with the double-ended mini-module. The selections of $4 <$ PWD < 6.43 and $6.5 <$ TD < 9.0 give the pion rejection factor of 4.85 with the 95% electron efficiency. 29

Energy	1 GeV	1.5 GeV	2.5 GeV	4 GeV
w/o PSD	14.0 ± 0.7	12.6 ± 0.6	9.7 ± 0.3	6.8 ± 0.2
w/o PSD (sim)	13.9 ± 0.4	11.9 ± 0.4	9.6 ± 0.3	7.4 ± 0.2
w/ PSD	14.7 ± 0.8	12.6 ± 0.7	9.5 ± 0.4	6.6 ± 0.4
w/ PSD (sim)	14.8 ± 0.4	11.8 ± 0.3	8.6 ± 0.3	7.1 ± 0.2

Table 1: The energy resolution σ_E/E (%) for electrons. The results of Monte Carlo simulation are also listed for comparison.

Energy	1 GeV	1.5 GeV	2.5 GeV	4 GeV
σ_x	6.9 ± 0.6	5.3 ± 0.6	4.4 ± 0.6	3.7 ± 0.6
σ_x (sim)	6.6 ± 0.2	5.8 ± 0.2	4.8 ± 0.2	3.8 ± 0.2
σ_y	6.2 ± 0.5	5.0 ± 0.5	4.5 ± 0.5	3.7 ± 0.5
σ_y (sim)	6.0 ± 0.2	5.8 ± 0.2	4.8 ± 0.2	3.6 ± 0.1

Table 2: The position resolution σ_x,σ_y (mm) for electrons.

Energy	1 GeV	1.5 GeV	2.5 GeV	4 GeV
w/o PSD	40.0 ± 1.3	32.5 ± 1.0	27.3 ± 0.7	22.2 ± 0.4
w/o PSD (sim)	36.1 ± 1.3	31.1 ± 1.0	28.2 ± 1.2	21.2 ± 0.8
w/ PSD	40.0 ± 1.5	34.6 ± 1.1	28.3 ± 0.7	24.4 ± 0.5
w/ PSD (sim)	36.6 ± 1.1	32.3 ± 1.0	29.0 ± 1.0	23.6 ± 1.0

Table 3: The energy resolution σ_E/E (%) for pions.

Electron efficiency	90%		95%		98%	
	Exp.	Sim.	Exp.	Sim.	Exp.	Sim.
PSD	11.9	12.2	10.6	10.2	8.56	8.50
C Value	26.6	26.0	14.7	18.6	7.89	12.0
S Value	31.1	28.1	18.7	18.2	10.9	11.7
PSD + C	$>$320	455	$>$190	278	119	200
PSD + S	$>$260	714	$>$260	455	202	208

Table 4: The pion rejection factor with various techniques. In case a small number of events were selected for experimental data, we set lower limits at the 95% C.L.. It was denoted by the symbol ”$>$”.

Electron efficiency	90 %	95 %	98 %
PWD	4.90	3.94	3.07

Table 5: The pion rejection factor with the LESFI modules. The PWD represents the method of the pulse widths.

Electron efficiency	90 %	95 %	98 %
PWD	2.95	2.29	1.91
TD	2.85	2.53	2.17
PWD + TD	6.90	4.85	3.20

Table 6: The pion rejection factor with the double-ended mini-module. The PWD represents the method of the pulse widths and TD indicates the method of the time difference.

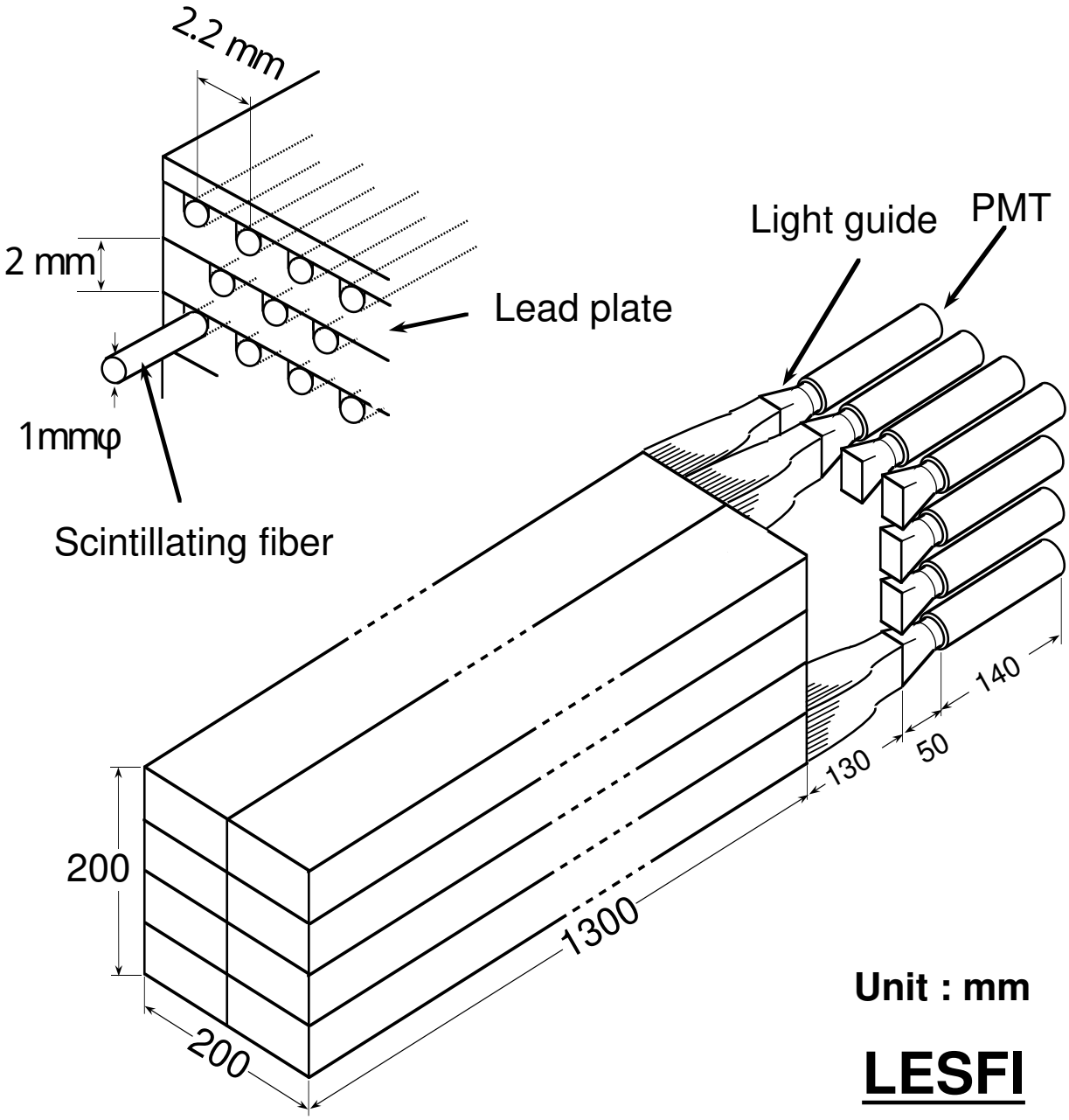

Figure 1: Schematic drawing of LESFI modules.

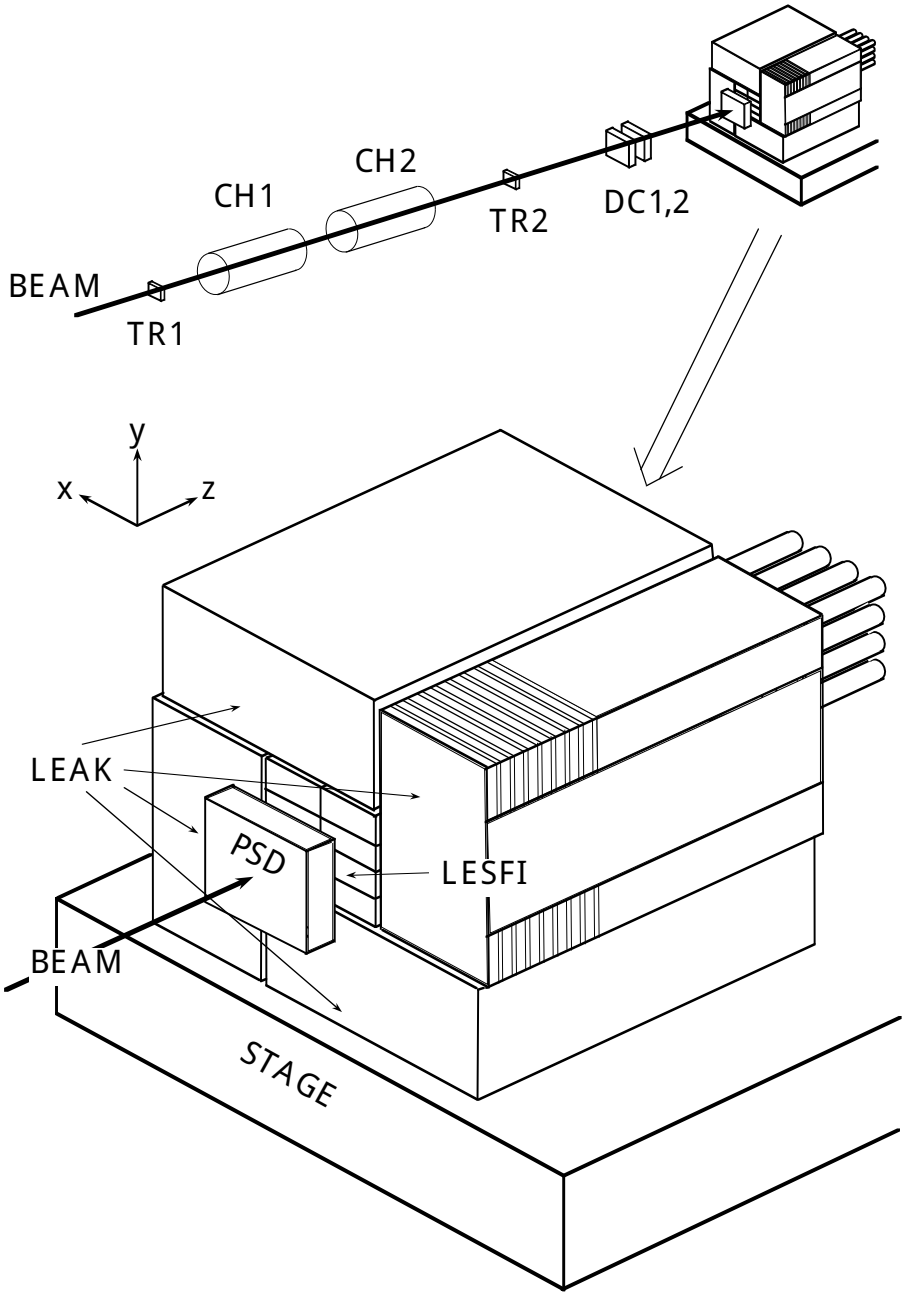

Figure 2: Setup of the beam test.

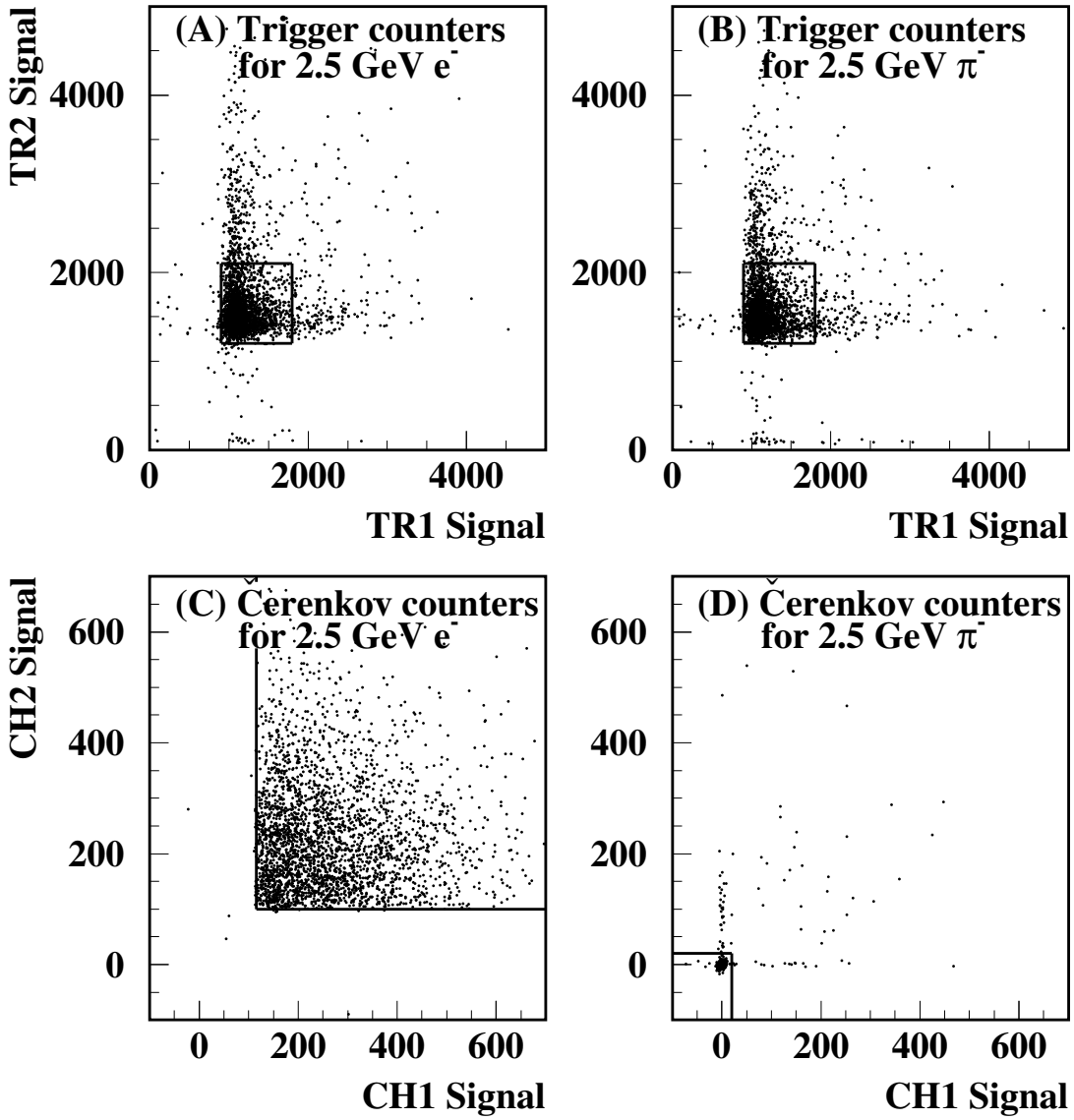

Figure 3: The scatter plots showing the signals of trigger counters (TR1 vs. TR2) for 2.5 GeV electrons (A) and pions (B). To remove the double track events we selected the rectangular region as shown in the figure. The scatter plots of gas Čerenkov signals (CH1 vs. CH2) for 2.5 GeV electrons (C) and pions (D) are also shown. The rectangular regions were selected to obtain higher purity.

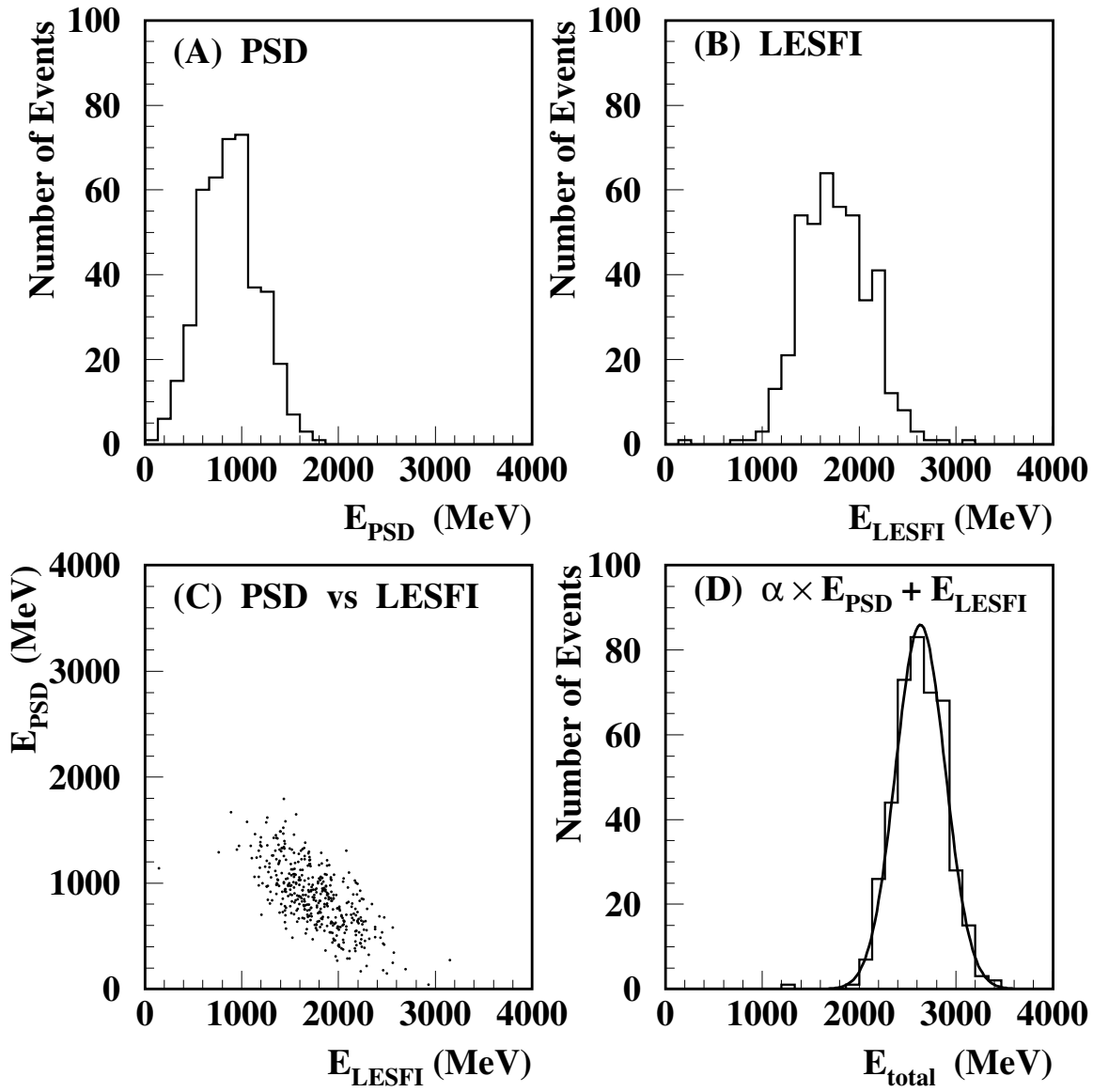

Figure 4: The energy distributions for 2.5GeV electrons with the incident angle of $\theta_x = 3°$. The PSD was located in front of LESFI modules. Shown are the energy distributions of the PSD (A) and the LESFI (B), the scatter plot of E_{PSD} versus E_{LESFI} (C) and the corrected total energy distribution (D).

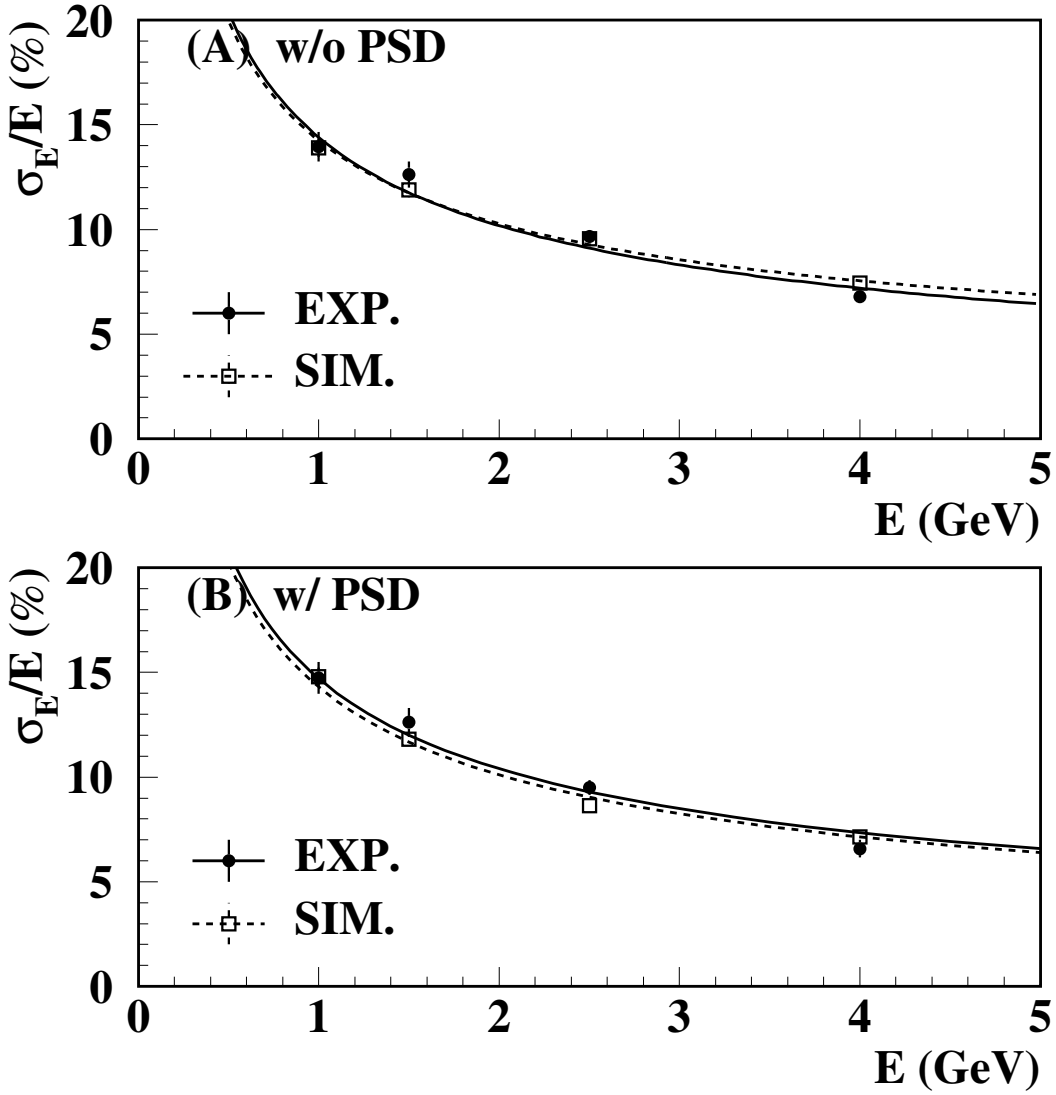

Figure 5: The energy resolution for electrons at $\theta_x = 3°$ without the PSD (A) and with the PSD (B). The filled circles and the solid line show experimental results, while the open squares and the dashed line show results of Monte Carlo simulations. Errors are statistical only.

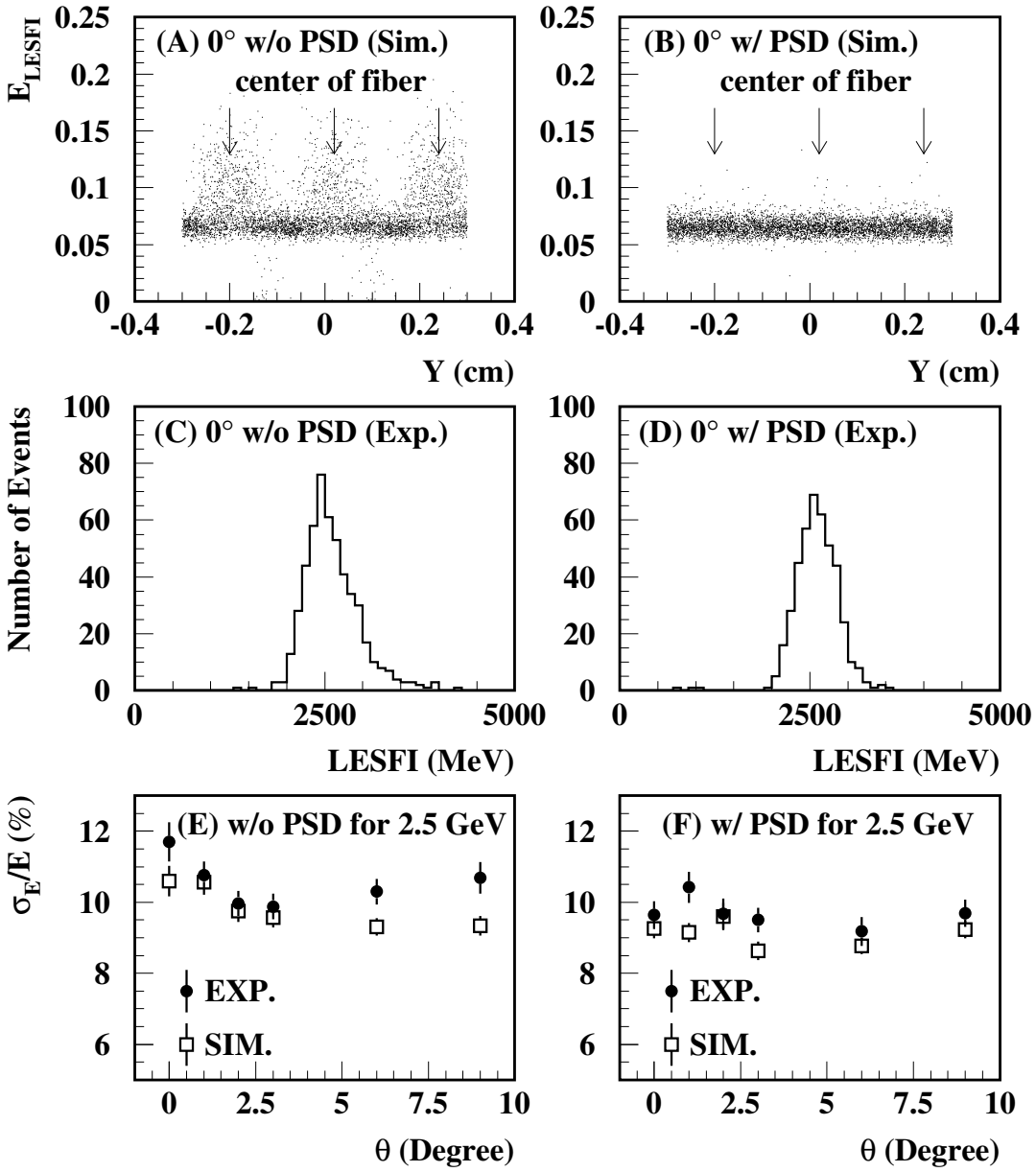

Figure 6: The scatter plots of Y-position versus E_{LESFI} by simulation at $\theta_x = 0°$ without the PSD (A) and with the PSD (B), the energy distributions of real data at $\theta_x = 0°$ without the PSD (C) and with the PSD (D) and angular dependence of the energy resolution without the PSD (E) and with the PSD (F). All of the data are for 2.5 GeV electrons.

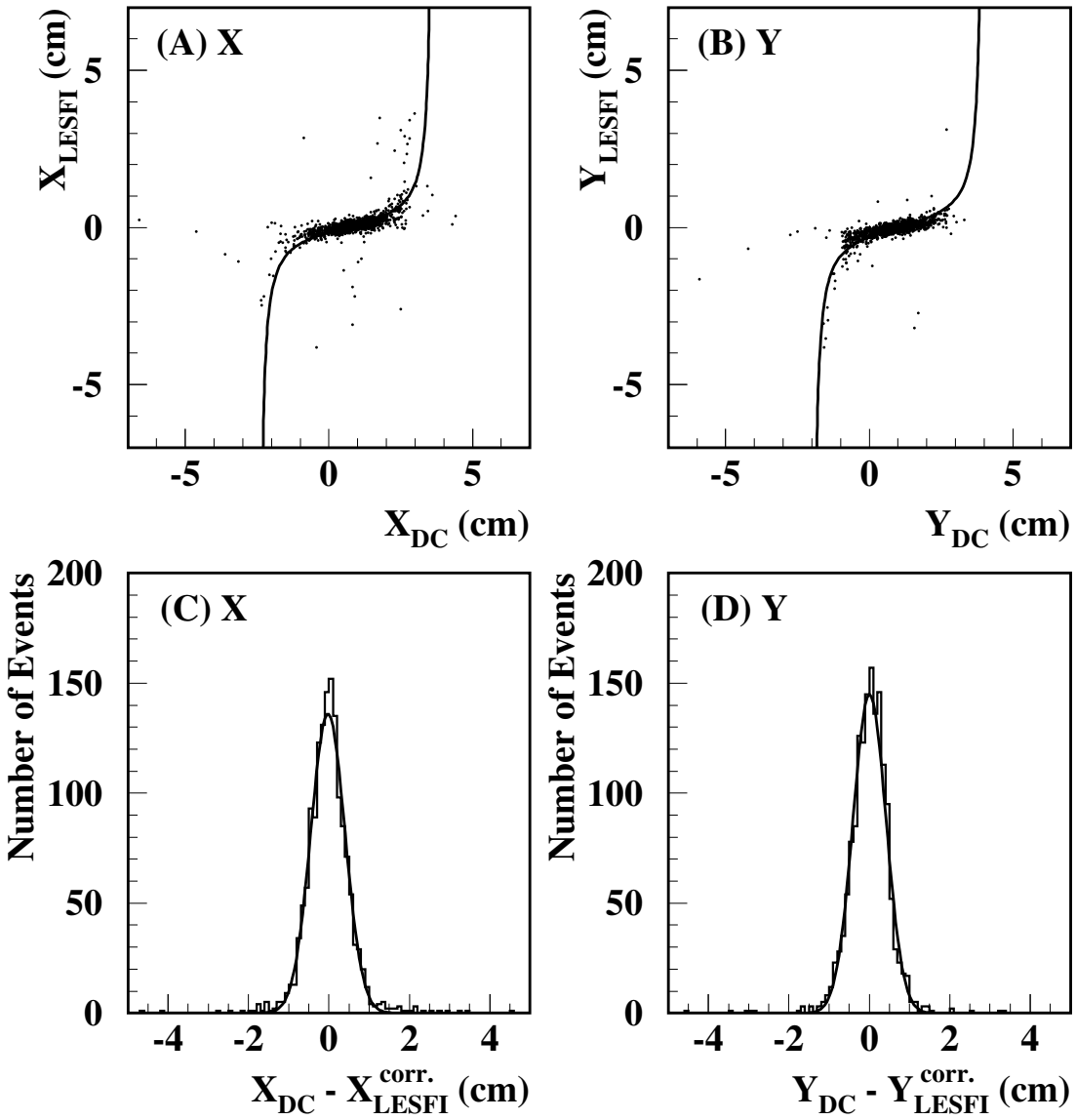

Figure 7: The scatter plots showing the position from the LESFI's data versus from the DC's data for x-coordinate (A) and y-coordinate (B). We use the data of 4 GeV electrons at $\theta_x = 3°$ without the PSD. The solid line is the fitting result with tangent-shape function. The residual distributions of corrected x-coordinate (C) and corrected y-coordinate (D) are also shown.

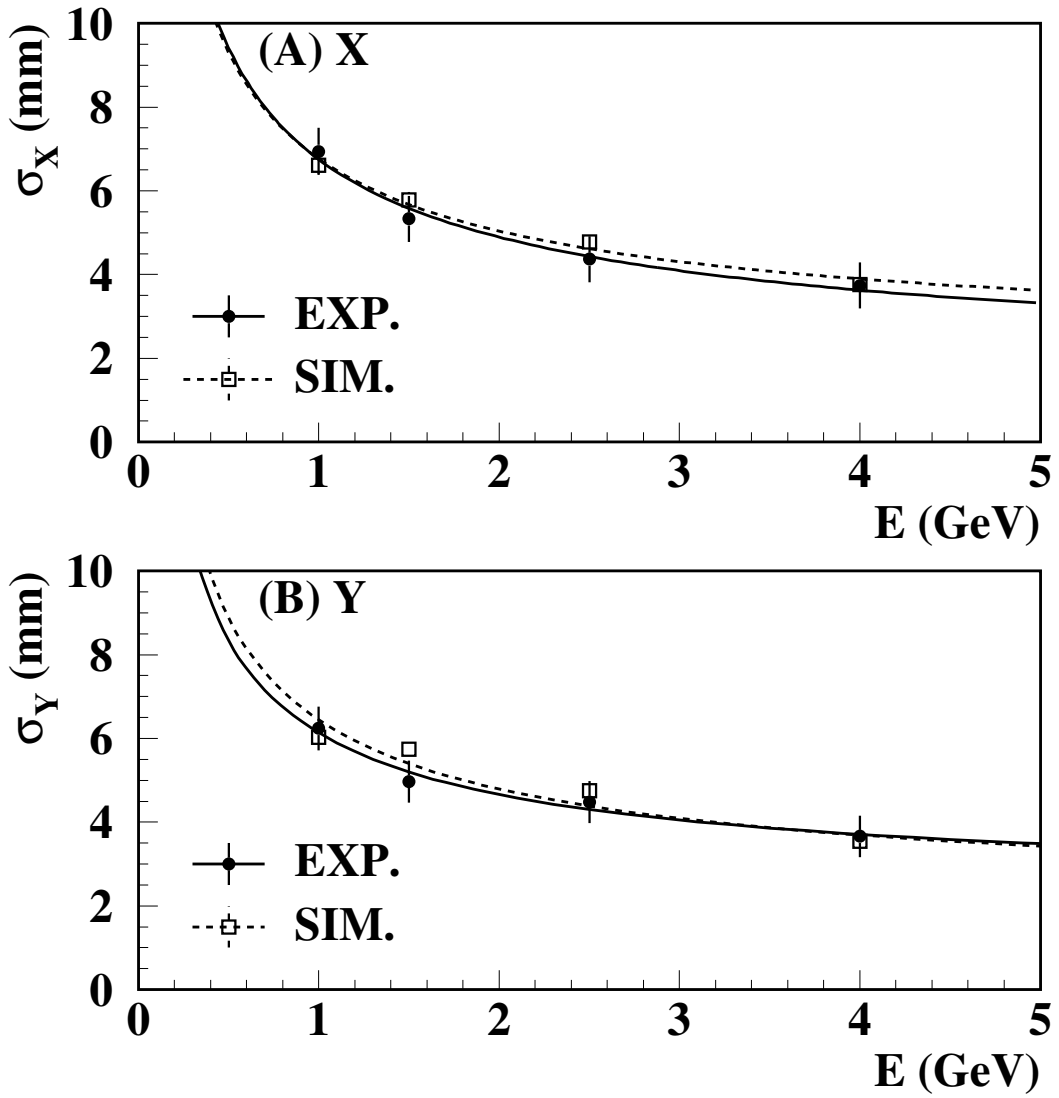

Figure 8: The position resolution for electrons with the incident angle of $\theta_x = 3^\circ$ without the PSD as a function of the incident energy. Shown are for x-coordinate (A) and y-coordinate (B). The filled circles and the solid line show experimental results, while the open squares and the dashed line show results of Monte Carlo simulations.

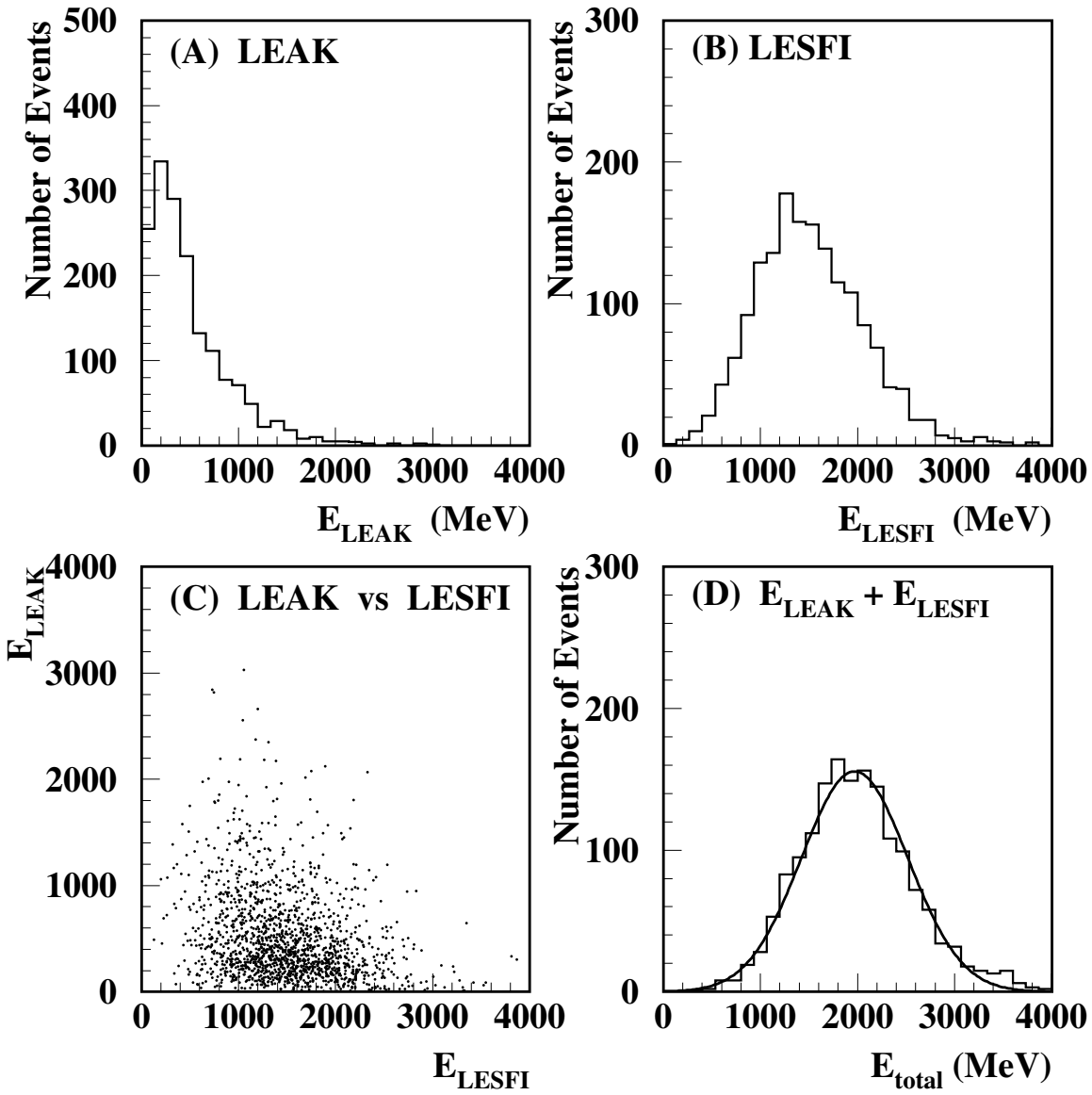

Figure 9: The energy distributions for 2.5GeV/c pions with the incident angle of $\theta_x = 0°$ without the PSD. Shown are the energy distribution of the LEAK (A) and the LESFI (B), the scatter plot of E_{LEAK} versus E_{LESFI} (C) and the combined energy distribution (D). The energy scale is normalized by electron data.

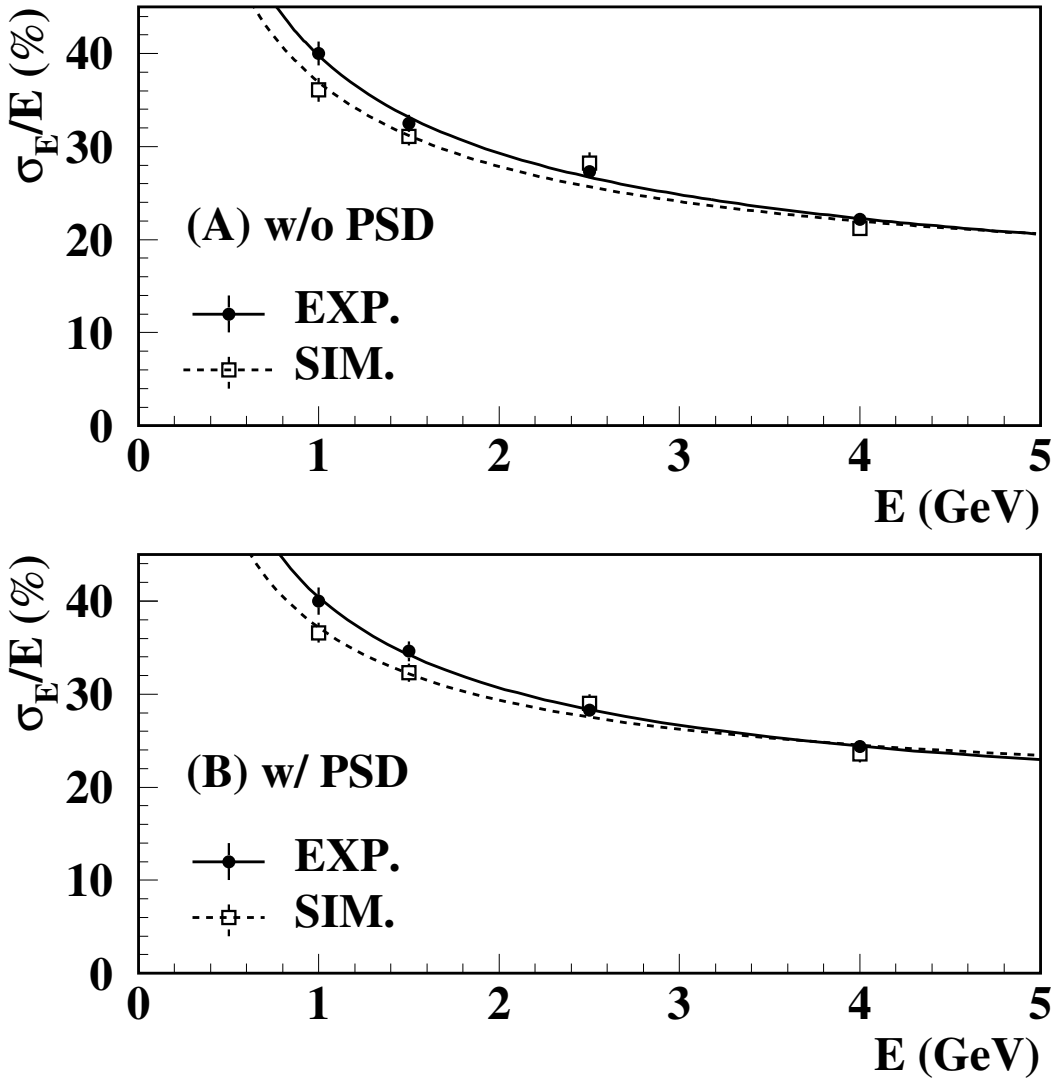

Figure 10: The energy resolution for pions at $\theta_x = 0^\circ$ without the PSD (A) and with the PSD (B). The filled circles and the solid line show experimental results, while the open squares and the dashed line show results of Monte Carlo simulations. The errors are statistical only.

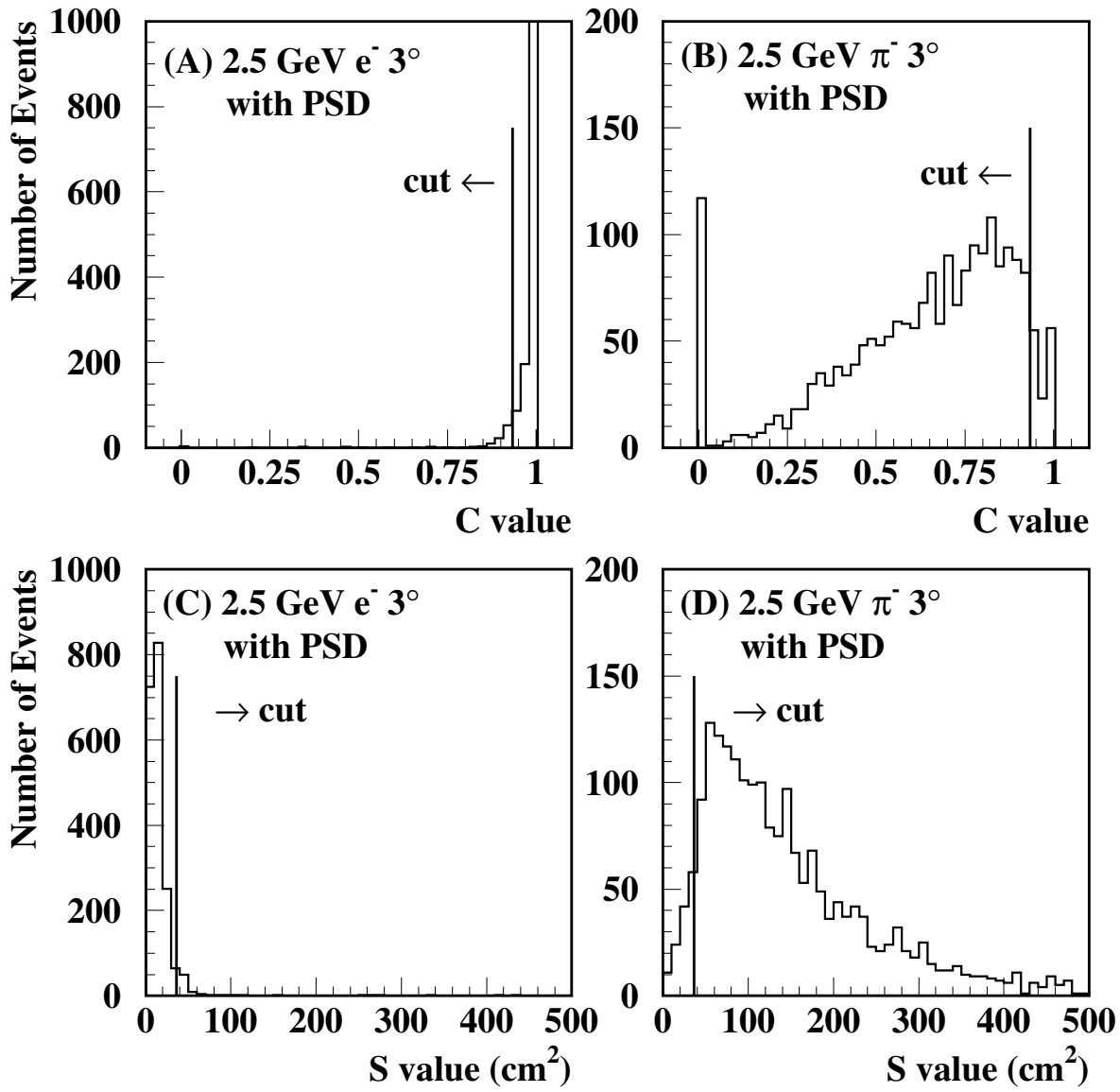

Figure 11: The distributions of the lateral shower spread for 2.5 GeV electrons and pions at $\theta_x = 3°$ with the PSD. Shown are C value (see text) for electrons (A), C value for pions (B), S value (see text) for electrons (C) and S value for pions (D). The selection of $C > 0.93$ gives the pion rejection factor of 14.7 with the 95% electron efficiency. The selection of $S < 36.1$ (cm^2) gives the pion rejection factor of 18.7 with the 95% electron efficiency.

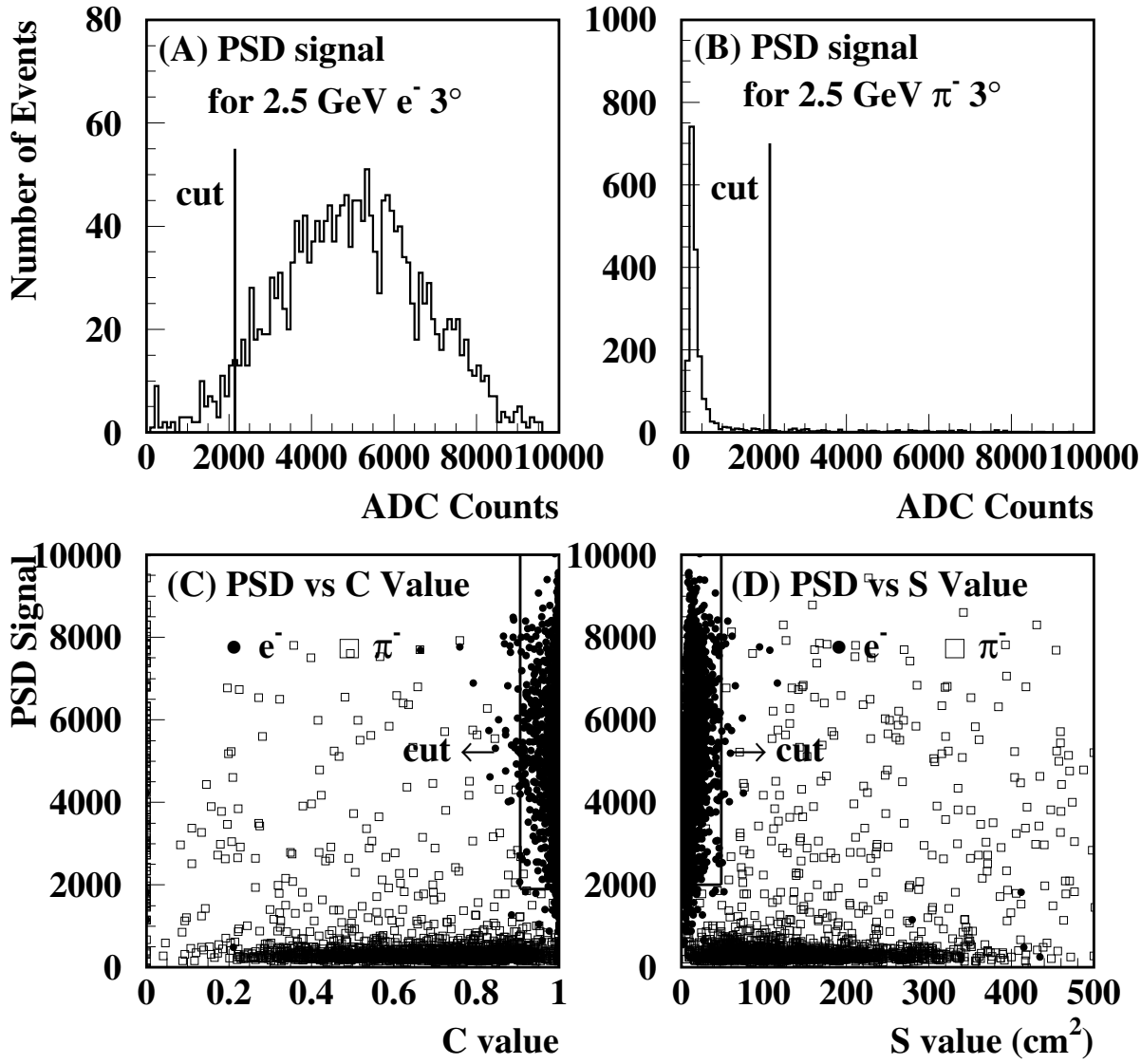

Figure 12: The pulse height distributions of the PSD for 2.5 GeV electrons (A) and 2.5 GeV pions (B). The pion rejection factor of 10.6 with the 95% electron efficiency can be obtained by the cut of PSD < 2150. Scatter plots of the PSD signal versus C value (C) and the PSD signal versus S value (D) are also given. The circle represents the electron data and the open square represents the pion ones. We use the data of 2.5 GeV electrons and pions at $\theta_x = 3°$. The selection of the PSD > 1000 and $C > 0.89$ gives the pion rejection factor of 118 with the 98% electron efficiency. The selection of the PSD > 2000 and $S < 48$ (cm^2) gives pion rejection factor of 202 with the 98% electron efficiency.

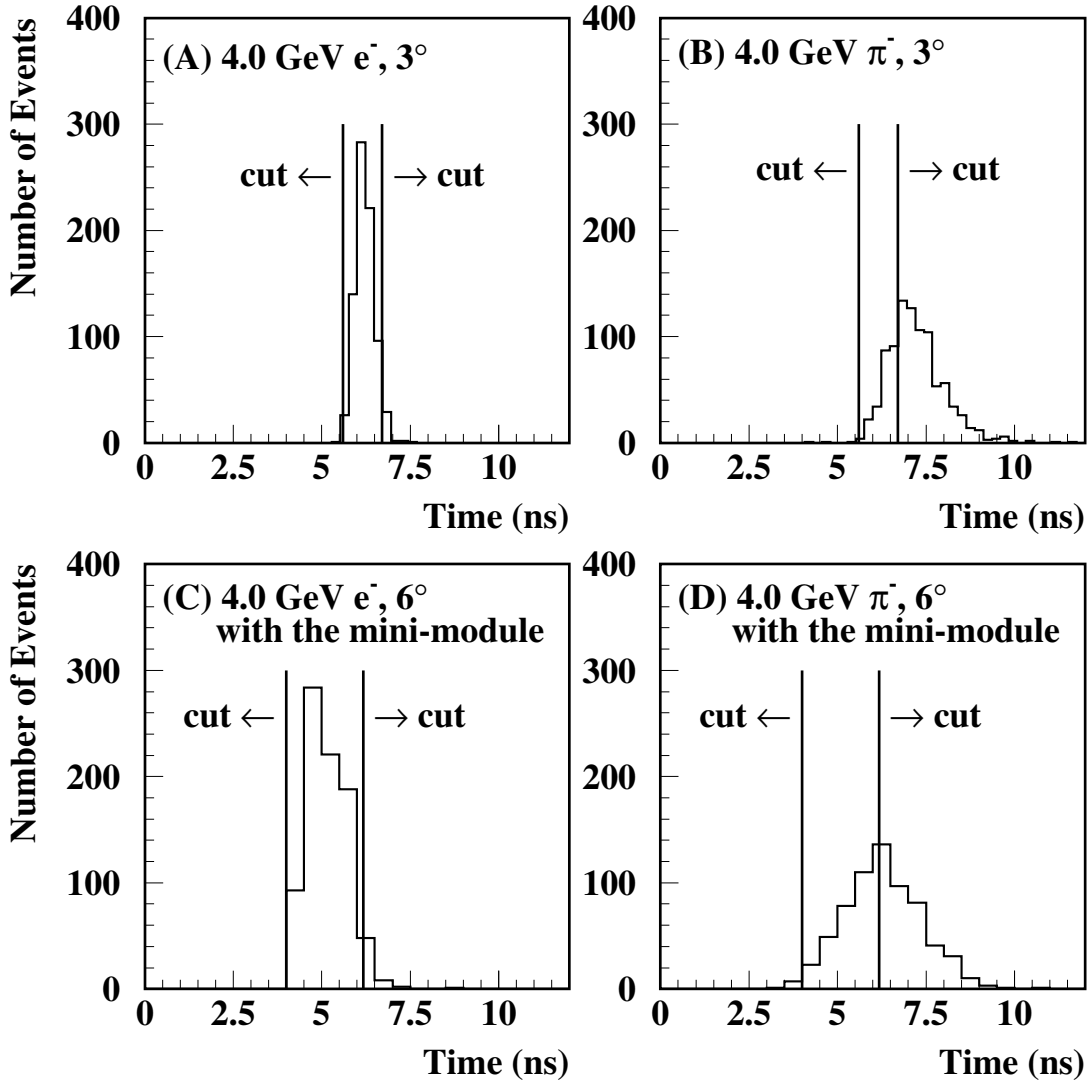

Figure 13: The distributions of the Pulse WiDths (PWD). The data were taken with the digital oscilloscope of 2GS/s. Shown are for 4.0 GeV electrons (A), for 4.0 GeV pions (B) with the ordinary LESFI modules, for 4.0 GeV electrons (C) and for 4.0 GeV pios (D) with the double-ended mini-module. The incident position and angle for the ordinary LESFI modules were the center of the segment and 3° in the horizontal plane. For the double-ended mini-module, the particles were incident to the edge with $\theta_x = 6°$. The selection of $5.6 <$ PWD < 6.7 for the LESFI modules gives the 4.1 pion rejection factor with the 95% electron efficiency. The selection of $4.0 <$ PWD < 6.17 for the double-ended mini-module gives the 2.29 pion rejection factor with the 95% electron efficiency.

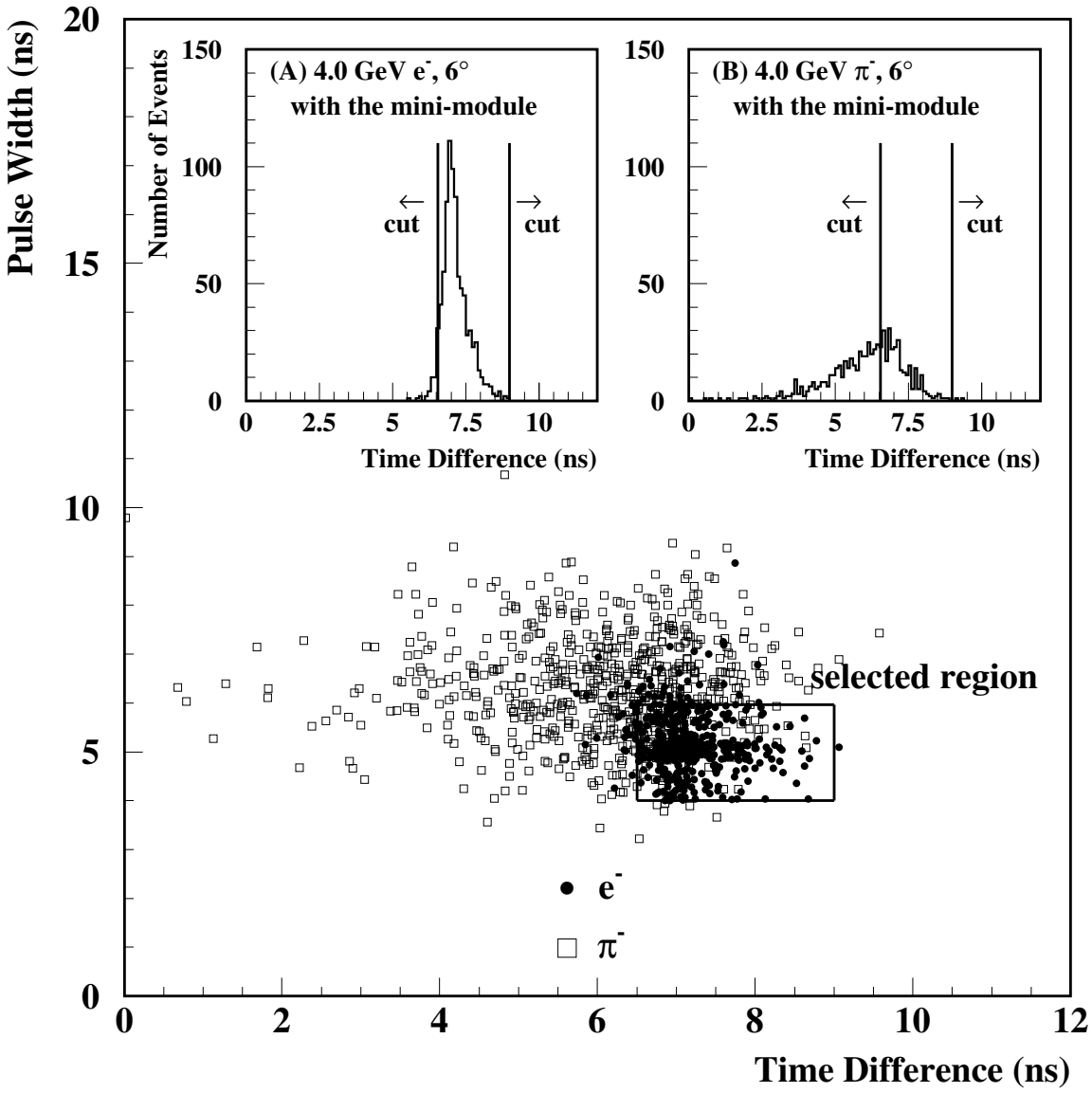

Figure 14: The distribution of Time Differences (TD) of the signals at the front end and the rear end with the double-ended mini-module. Superposed figures are for 4.0 GeV electrons (A) and for 4.0 GeV pions (B). The selection of $6.55 < \mathrm{TD} < 9.0$ gives the pion rejection factor of 2.53 with the 95% electron efficiency. The scatter plot shows the Pulse WiDths (PWD) versus the Time Differences (TD) with the double-ended mini-module. The selections of $4 < \mathrm{PWD} < 6.43$ and $6.5 < \mathrm{TD} < 9.0$ give the pion rejection factor of 4.85 with the 95% electron efficiency.